Journal of Optoelectronics and Advanced Materials Vol. 2, March 2000, p. 31-42

ANALYSIS OF TIME-OF-FLIGHT PHOTOCURRENTS IN a-Si:H DEPOSITED BY EXPANDING THERMAL PLASMA

G. J. Adriaenssens, H.-Z. Song, V. I. Arkhipov, E. V. Emelianova, W. M. M. Kessels[a], A. H. M. Smets[a], B. A. Korevaar[a], M. C. M. van de Sanden[a]

Laboratorium voor Halfgeleiderfysica, Universiteit Leuven, Celestijnenlaan 200D, 3001 Leuven-Heverlee, Belgium
[a]Department of Applied Physics, Eindhoven University of Technology, P.O. Box 513, 5600 MB Eindhoven, The Netherlands

The drift mobility of electrons and holes was studied in a standard time-of-flight (TOF) experiment, as a function of temperature and applied electric field, for several series of a-Si:H samples that were deposited at high growth rate in an expanding thermal plasma (ETP) at substrate temperatures near 400 °C. Room-temperature electron mobilities are somewhat lower than for standard plasma-enhanced chemical vapor deposited (PECVD) material, but the hole mobility is more than one decade higher. The dispersion of the photocurrent transients is comparable to the one in PECVD samples, but both electron and hole mobilities of the ETP material are remarkably insensitive to the magnitude of applied electric fields in the measured range of 0.1 to 5.0×10^4 V/cm. The temperature dependence of the mobilities, on the contrary, is high, with resolved activation energies of ~0.24 eV for electrons and ~0.40 eV for holes. Standard multiple-trapping analysis of the above results in terms of the underlying density of localized states suggests rather wide distributions of tail states on both sides of the gap. To account simultaneously for the weak field dependencies it is necessary to consider non-negligible recombination or deep trapping of the carriers. Measurements and analysis of the post-transit TOF signals do support the presence of a strong deep-trapping component in the transient signal.

(Received February 17, 2000; accepted March 1, 2000)

Keywords: Hydrogenated amorphous silicon, Transient photocurrent, Drift mobility

1. Introduction

Hydrogenated amorphous silicon (a-Si:H) has in recent years proved to be very amenable to technological applications such as non-crystalline solar cells and thin-film transistors. Still, an alternative for the slow film deposition rate of 0.1–0.3 nm/s of the standard plasma-enhanced chemical vapor deposition (PEVCD) process would be advantageous, especially with respect to solar cell usage, where hundreds-of-nanometer thick intrinsic layers need to be grown. Amongst the techniques that have been investigated for this purpose, film production in an expanding thermal plasma (ETP), which belongs to the so-called remote plasma methods, was found to produce good-quality a-Si:H at deposition rates of up to 10 nm/s [1]. In addition, it was observed that the ETP a-Si:H films do exhibit a hole drift mobility which is more than a factor of 10 higher than the one measured in device-quality PECVD samples, while at the same time the electron drift mobility is reduced by not more than a factor 3 to 6 [2]. These ETP mobilities, and specifically the high value of the hole drift mobility, further contribute to making this deposition technique attractive for solar cell applications.

The specific distributions of electronic states that lead to the above-mentioned differences in carrier mobility between the ETP material and reference PECVD samples, can be investigated by further analysis of the *time-of-flight* (TOF) transient photocurrents that already have served to deduce

the drift mobilities to begin with [3]. Data sets over wide ranges of time, temperature, and applied electric field are required for this purpose, and are analyzed within the well-established frame of the multiple-trapping transport. However, a first tentative application of these standard procedures to the ETP samples did lead to apparent internal contradictions with respect to the width of the localized states distribution. In this contribution we will, therefore, present the experimental situation involving the ETP deposition and the generation of the TOF data, examine the basic tenets of the multiple-trapping formalism, and see how the experimental results can be reconciled with the theoretical considerations.

2. Sample preparation and measurement set-up

The a-Si:H samples used in this study are sandwich structures with a bottom Cr substrate on glass and a series of top semi-transparent Cr contacts evaporated in high vacuum. The a-Si:H layer is deposited on the Cr-covered substrate in a remote plasma deposition chamber as illustrated in Fig. 1.

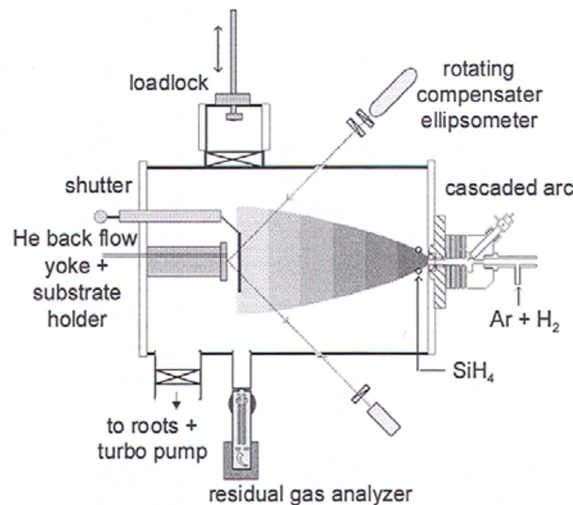

Fig. 1. Schematic diagram of expanding thermal plasma (ETP) deposition system.

Briefly: The arc plasma of a Ar and H_2 mixture is allowed to expand into a large vessel, where the SiH_4 gas is injected into the plasma background. Different from PECVD or other remote-plasma techniques, in which SiH_4 is decomposed by electronic kinetics, this technique has as its main deposition reaction:

$$H + SiH_4 \rightarrow SiH_3 + H_2.$$

The substrate temperature is normally higher than that of PECVD, but the main characteristic is the high deposition rate of about 10 nm/s, which is 10 - 100 times that of PECVD. The samples for this study were grown with substrate temperatures varying from 300 to 450 °C, and with deposition rates from 2.5 to 12 nm/s.

The drift mobilities and the density ot states (DOS) distribution of gap states were measured with a standard time-of-flight setup. Strongly absorbed light from a nitrogen-laser pumped dye laser with 3 ns pulse duration and ~530 nm wavelength creates free electrons and holes just behind the semi-transparent and electrically blocking Cr contact. An externally applied electric field will then, depending on its polarity, cause either the electrons or the holes to drift to the other electrode where they will be collected. The time it takes a representative set of carriers to reach that collecting electrode is called the *transit time.* A HP 214B pulse generator is used as the bias voltage source for times up to 10 ms and a DC voltage supply is used for longer times (up to 5 s in practice). The transient photocurrent is monitored with an IWATSU-8123 digitizing storage oscilloscope and the

data are subsequently transferred to a computer, which also controls the timing of the pulses. During measurements, the temperature is controlled at a fixed value by a combination of liquid nitrogen cooling or electrical heating of the support rod of the sample.

3. Experimental results

Fig. 1 shows a set of TOF transient photocurrent curves for a typical sample on the traditional double-logarithmic scales. The initial peaks are the RC response of the setup. On each curve, the transit time, t_T, is indicated by the intersection point of the extrapolated pre- and post-transit parts of

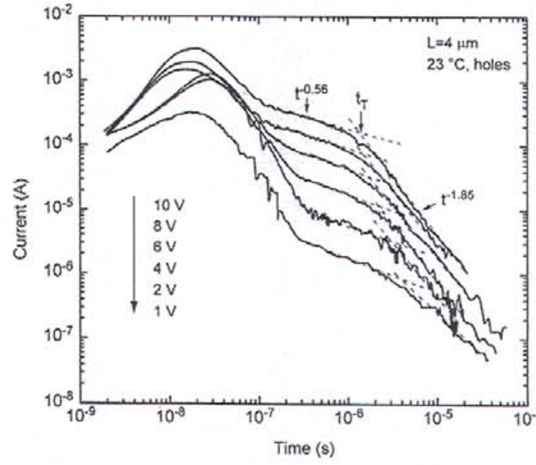

Fig. 2. Typical room temperature TOF hole transient from a sample prepared at 450°C, at a deposition rate of 11 nm/s. Dashed lines show the power laws describing the pre- and post-transit currents.

the current trace which, respectively, can be described by:

$$t^{-(1-\alpha_1)} \quad \text{for } t < t_T,$$
$$t^{-(1+\alpha_2)} \quad \text{for } t > t_T.$$

This power-law behavior of the current is in agreement with the notions of the so-called dispersive transport in amorphous semiconductors, which can be modeled by the process of multiple-trapping transport in a (more or less) exponentially decreasing density of states [3,4]. Fig. 1 illustrates that the transit time clearly shifts with the applied electric field, and that the dispersion parameters α_1 and α_2 are independent of the field. These are essential signs for meaningful TOF measurements. Similar results are observed under other conditions and in other samples. Accordingly, the ETP material under study appears to be of good quality. The temperature dependence of the dispersion parameters was found to be analogous to the one reported for PECVD a-Si:H [5]: At lower temperatures $\alpha_1 > \alpha_2$, but α_2 increases faster with increasing temperature than α_1, leading to values of $\alpha_1 \cong 1$ and $\alpha_2 > 1$ at higher temperatures.

From the measured transit time t_T, the carrier drift mobility can be calculated according to

$$\mu_d = L^2 / t_T V\,, \tag{1}$$

where L is the sample thickness and V the voltage applied across the sandwich structure. A representative set of drift mobility data are shown, connected by full lines, against the reciprocal temperature for a typical ETP sample in Fig. 3. For comparison, literature data from standard PECVD a-Si:H [6,7] are also shown. With respect to the results of the PECVD material, the drift mobility of electrons (μ_{de}) is lower, while the hole mobility (μ_{dh}) is higher. Detailed comparisons show that, at room temperature, μ_{dh} is some 10 times higher in ETP than in PECVD samples, while μ_{de} is a factor 3

to 4 lower at 250 K. The trend is towards a lessening of the latter difference towards room temperature, but thicker TOF samples would be required to confirm this. In addition, the μ_d of the ETP sample is only weakly dependent on, or even independent of, the electric field in the range of 0.5-2.5 × 10^4 V/cm. This is quite different from the clear field dependence of μ_d that is well-documented [8] for standard a-Si:H, and that can also be observed with the literature data in Fig. 3. Finally, as for PECVD samples, the μ_d is thermally activated at lower temperatures:

$$\mu_d = \mu_{d0} \exp(-\frac{E_a}{kT}), \tag{2}$$

but with an activation energy E_a that is virtually independent of the electric field. In detail: for μ_{de}, $E_a \approx 0.24$ eV, which is high with respect to typical PECVD value of 0.15 eV, while for μ_{dh} a value of 0.39 eV is measured, which is close to the standard values of 0.35 - 0.4 eV. The results shown in Fig. 3 are representative for a whole set of measured ETP samples, but with individual fluctuations in the precise amount by which μ_{dh} is higher, or μ_{de} lower, or E_a changed.

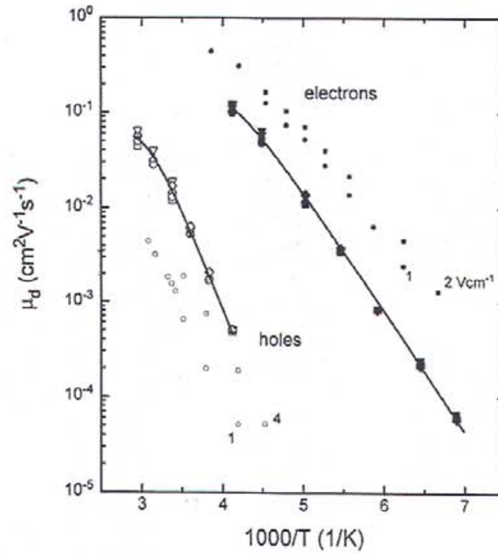

Fig. 3. Temperature dependence of the drift mobilities of electrons and holes with electric fields of 0.5, 1.0, 1.5, 2.0 and 2.5 × 10^4 V/cm across the sample of Fig. 2. Also shown, by smaller symbols and without connecting line, are data (for indicated fields × 10^4) from Refs. 6 and 7.

Within the framework of the multiple-trapping model, and as outlined in the next section, charge that is trapped at an energy deeper than $E_T = kT \ln(\nu_o t_T)$, where k is the Boltzmann constant and ν_o the attempt-to-escape frequency, will only contribute to the current at times $t \gg t_T$ and then (ideally) leave the sample without further retrapping. Under the standard assumption of energy independent capture cross-section, the post-transit emission current will thus be proportional to the number of carriers released from the traps, and hence to the DOS $g(E)$. Seynhaeve *et al.* [9] deduced a simple formula to relate the transient photocurrent $I(t)$ to the density of gap states $g(E)$:

$$I(t) \cdot t = \frac{Q_0 \nu_0 t_0}{2g(0)} g(E), \quad E = kT \ln(\nu_0 t), \tag{3}$$

where Q_0 is the total charge participating in the transient current, t_0 the free-carrier transit time, and $g(0)$ the value of the DOS at the mobility edge. It is obvious that by measuring over the widest possible time domain, the optimum information on the DOS will be obtained.

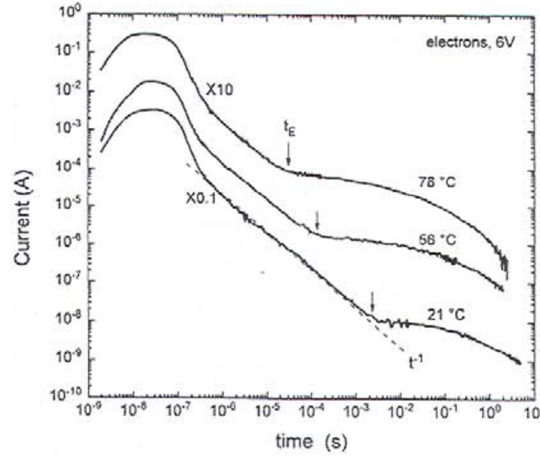

Fig. 4. Transient photocurrent traces in the post-transit regime, from the sample of Fig. 2, at different temperatures. t_E marks the start of emission from the deep traps.

Fig. 4 shows examples of the post-transit electron photocurrent at different temperatures for a typical ETP sample. The post-transit currents are essentially field-independent. The t^{-1} part of the decay is probably indicative of a pronounced dangling-bond D^- peak in the mid-gap DOS, similar to what was seen in the simulations with a deep defect by Silver *et al.* [10], while the deviation from t^{-1} at longer times marks the onset of carrier emission from that midgap trap [11]. These points are indicated on each curve as t_E. Since the t_E correspond in each instance to an identical energy, we can use it together with the $E = kT \ln(\nu_o t)$ relationship to determine ν_o.

In order to calculate the magnitude of the DOS, a few more parameters of Eq. (3) have to be determined. Q_0 is estimated by integrating the current at the highest measurement temperature up to the end of the measurement. Due to experimental limits in temperature and time, it will still be less than it should be and hence lead to some over-estimation of $g(E)$. From Fig. 3, μ_0 is expected to be close to or slightly lower than the standard value for PECVD a-Si:H. So we assume μ_0 to be roughly equal to that value: 8 $cm^2V^{-1}s^{-1}$. For $g(0)$ we take 10^{21} $cm^{-3}eV^{-1}$ as is often used for a-Si:H. With these parameters, the DOS distribution of deep electron traps shown in Fig. 5 is calculated. We see that the three profiles obtained at different temperatures match each other, which validates the resolved curve as representing the true DOS. It is thus seen that the midgap electron trap of ETP a-Si:H is located some 0.8 eV below the conduction mobility edge, with an approximate maximum density of 7×10^{16} $cm^{-3}eV^{-1}$. The integrated density of this trap is 6.4×10^{15} cm^{-3}. These results are similar to the anologous ones from PECVD a-Si:H, except maybe that the trap is located a bit deeper here [11]. However, the background DOS between the band tail and the midgap states, is nearly three orders of magnitude below the density of the midgap trap while only one order of magnitude difference is observed in the case of PECVD a-Si:H [11].

The distribution of localized states on the valence band side of the gap was resolved in the same way as described above for the conduction band side. The midgap hole trap is found situated some 0.8-0.9 eV above the valence band edge. With estimates for Q_0, ν_0, μ_0 and $g(0)$ as outlined above, the resolved density of midgap hole traps is about 5×10^{16} cm^{-3}. Again we found a strong decrease in the DOS in the region between the band tail and the midgap trap. In fact, similar DOS distributions to the ones above were observed in all measured ETP a-Si:H samples. The total density of the midgap trap is always more or less 10^{16} cm^{-3}, and the background DOS is at least one hundred times lower than the density of the midgap states.

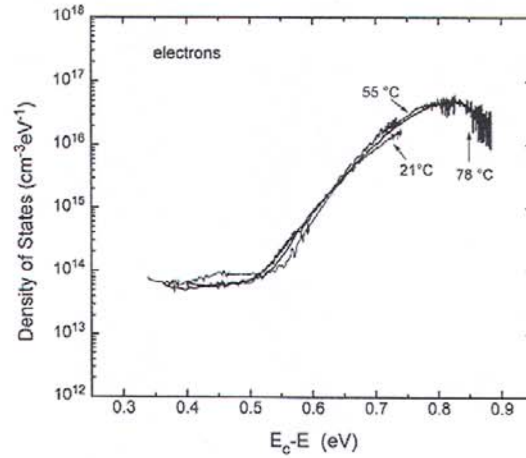

Fig. 5. Density of localized electron states derived from the post-transit photocurrents of Fig. 4, with $Q_0 = 7.2\times10^{-7}$ C, $\mu_0 = 8$ cm^{2}V^{-1}s^{-1}, $\nu_o = 2.2\times10^{12}$ s^{-1}, $g(0) = 10^{21}$ cm^{-3}eV^{-1}.

4. Analysis and interpretation

4.1. Initial evaluation

From the earliest evaluations of the anomalously dispersive multiple-trapping carrier transport that governs the behavior of transient photocurrent signals in amorphous semiconductors [12,13], it was realized that the instantaneous fraction of free to trapped charge defined the experimentally observed drift mobility with respect to the conceptual free-carrier mobility μ_0:

$$\mu_d(t) = \frac{n_f(t)}{n_t(t) + n_f(t)}\mu_0, \tag{4}$$

where n_f and n_t are the free and trapped excess carrier densities in the sample. When using Eq. (1), one takes the carrier distribution at $t = t_T$ as reference point. In comparing the TOF results of ETP and PECVD samples, it may then be concluded that the trap density will be lower in ETP a-Si:H on the valence band side, and in PECVD material on the conduction band side, always over the energy range where it can influence the transit time. This energy range should roughly correspond to the observed activation energy of the drift mobility [14], *i.e.* over at least as wide a range in ETP as in PECVD material. However, this immediately leads to a contradiction within the assumptions of the simple multiple-trapping formalism that traditionally serves to evaluate the TOF results: We should expect comparable field dependencies of the drift mobility in samples from either origin, yet virtually no applied field dependence can be resolved in the ETP a-Si:H. In the next sections, it will be shown that this contradiction can be resolved by taking into consideration monomolecular recombination, *i.e.* deep trapping, of travelling carriers.

4.2. Non-equilibrium energy distribution of localized carriers

Since the presence of a broad DOS distribution is inherent in disordered systems, charge carrier transport and recombination in these materials normally occur under the condition of a non-equilibrium energy distribution of localized carriers. Before thermalization is finished, the effective trap-controlled mobility of photogenerated carriers decreases with time giving rise to smoothly decreasing dispersive transient photocurrents observed in TOF and transient photoconductivity (TP) measurements.

Before an equilibrium distribution of localized carriers within the DOS distribution is established, most carriers occupy metastable states from which carrier release remains improbable until the time t. Since the average carrier release time, t_r, from a localized state of the energy E is

$$t_r = \frac{1}{\nu_0}\exp\left(\frac{E}{kT}\right), \tag{5}$$

the probability, w_m, for this state to be a metastable one until the time t is determined by the Poisson distribution as

$$w_m(E,t) = \exp\left(-\frac{t}{t_r}\right) = \exp\left[-\nu_0 t\exp\left(-\frac{E}{kT}\right)\right]. \tag{6}$$

The density of metastable states, $g_m(E,t)$, is the product of the total density of states, $g(E)$, and the probability for a given state to be metastable at the time t:

$$g_m(E,t) = g(E)w_m(E,t) = g(E)\exp\left[-\nu_0 t\exp\left(-\frac{E}{kT}\right)\right]. \tag{7}$$

Since the density of carriers localized in metastable states, $\rho_m(E,t)$, changes only due to trapping the function $\rho_m(E,t)$ must be proportional to the density of metastable states as,

$$\rho_m(E,t) = f(t)g_m(E,t), \tag{8}$$

where $f(t)$ is the occupational probability. Note that Eq. (8) is written under the conventional assumption of the energy-independent carrier cupture cross-section. Integrating Eq. (8) over energy yields the total carrier density, $p(t)$, as,

$$p(t) = f(t)\int_0^\infty dE\, g_m(E,t). \tag{9}$$

Since the occupational probability of metastable states changes only due to the trapping of free carriers, the following equation governs the function $f(t)$:

$$\frac{df(t)}{dt} = c_0 p_c(t) = \frac{1}{\tau_0 N_t}p_c(t), \tag{10}$$

where c_0 is the carrier capture cross-section, τ_0 the lifetime of free carriers before trapping, and N_t the total density of localized states. Eliminating $f(t)$ from Eqs. (9) and (10) yields an equation relating the total carrier density to the density of free carriers under the non-equilibrium (dispersive) transport regime:

$$p_c(t) = \frac{d}{dt}\left[\tau(t)p(t)\right], \tag{11}$$

with the function $\tau(t)$ determined as

$$\tau(t) = \tau_0 N_t\left[\int_0^\infty dE\, g_m(E,t)\right]^{-1} = \tau_0 N_t\left\{\int_0^\infty dE\, g(E)\exp\left[-\nu_0 t\exp\left(-\frac{E}{kT}\right)\right]\right\}^{-1}. \tag{12}$$

The exponential term in the integrand of Eq. (12) represents a very steep function of the energy at around the so-called demarcation energy, $E_d(t) = kT\ln(\nu_0 t)$, that allows the following approximation for this function:

$$\exp\left[-\nu_0 t \exp\left(-\frac{E}{kT}\right)\right] \cong \begin{cases} 0 , & E < E_d(t) , \\ 1 , & E > E_d(t) . \end{cases} \quad (13)$$

Substituting Eq. (13) into Eq. (12) reduces the latter equation to

$$\tau(t) = \tau_0 N_t \left[\int_{E_d(t)}^{\infty} dE \, g(E) \right]^{-1} . \quad (14)$$

Equation (11) together with Eq. (12) form the basis for consideration of carrier transport and recombination phenomena under the non-equilibrium (dispersive) conditions. Note that this equation remains valid if both carrier drift and recombination occur simultaneously. In particular, this makes possible the use of Eq. (11) in problems with coordinate-dependent carrier densities. Traditionally, recombination is not considered to play a role in the TOF experiment, while in the transient photoconductivity (TP) experiment, where both electrons and holes do move in a gap-cell geometry, trap controlled recombination will be responsible for the kink in a $\log j$ *vs* $\log t$ curve. The latter is then independent of the applied electric field. In the following section, the above equations will be applied to the consideration of the dispersive carrier transport and recombination under the TOF experimental conditions.

4.3. Small-signal dispersive carrier drift and recombination in a homogeneous field

The multiple-trapping model is based on the assumption that charge transport in a disordered material is maintained only by carriers occupying extended states. This approach implies the following form of the continuity equation for the charge carrier density:

$$\frac{\partial p(x,t)}{\partial t} + \frac{\partial j_c(x,t)}{\partial x} = 0 , \quad (15)$$

where j_c is the conduction current density. At a first glance, Eq. (15) does not account for carrier recombination. However, only monomolecular recombination of injected charge carriers is feasible under TOF conditions and this recombination mode is equivalent to carrier trapping by sufficiently deep localized states from which carriers cannot be released at times shorter than the longest experimental transit time. The deep trapping can be accounted for by incorporating deep traps into the DOS distribution in Eqs. (12) and (14).

Under the dispersive transport conditions, a spreading of the carrier density is caused by shallow trapping rather than by diffusion. This makes it feasible to neglect the diffusion term in the conduction current density such that the latter takes the form

$$j_c(x,t) = \mu_c F p_c(x,t) . \quad (16)$$

Substituting Eqs. (11) and (16) into Eq.(15) yields,

$$\frac{\partial p(x,t)}{\partial t} + \mu_c F \frac{\partial^2}{\partial x \partial t}\left[\tau(t) p(x,t)\right] = 0 . \quad (17)$$

Integrating Eq. (17) over the time and taking into account the initial condition $p(x,0) = 0$ leads to the following dispersive transport equation:

$$p(x,t) + \mu_c F \tau(t) \frac{\partial}{\partial x} p(x,t) = 0 . \quad (18)$$

Finally, solving Eq. (18) yields

$$p(x,t) = A(t) \exp\left[-\frac{x}{\mu_c F \tau(t)}\right] . \quad (19)$$

It is assumed in Eq. (19) that carriers are generated at the front surface $x = 0$. The function $A(t)$ may then be found by normalizing the total density of carriers. Integrating the carrier density over the coordinate from $x = 0$ to $x = \infty$ must yield the surface density of generated carriers, σ. This procedure leads to the following function $A(t)$:

$$A(t) = \frac{\sigma}{\mu_c \tau(t)} . \tag{20}$$

Substituting Eq. (20) into Eq. (19) yields as a universal expression for the carrier packet shape,

$$p(x,t) = \frac{\sigma}{\mu_c F \tau(t)} \exp\left[-\frac{x}{\mu_c F \tau(t)} \right], \tag{21}$$

which is independent of the specific choice of the function $\tau(t)$, i.e. of the specific choice of the DOS distribution. Under small-signal conditions, the TOF transient current, $j(t)$, may be calculated by averaging the conduction current, $j_c(x,t)$, over the spatial coordinate:

$$j(t) = \frac{1}{L} \int_0^L dx\, j_c(x,t) = \frac{e\mu_c F}{L} \int_0^L dx\, p_c(x,t) , \tag{22}$$

where L is the thickness of the sample. Substitution of Eqs. (11) and (21) into Eq. (22) then leads to an equation that relates the transient current to the function $\tau(t)$ as

$$j(t) = \frac{e\sigma\mu_c F}{L} \frac{d}{dt} \left(\tau(t) \left\{ 1 - \exp\left[-\frac{L}{\mu_c F \tau(t)} \right] \right\} \right) . \tag{23}$$

This transient current reveals two asymptotic forms. At shorter times, $\mu_c F \tau(t) << L$, one may neglect the exponential term in Eq. (23) and obtain the following expression:

$$j(t) = \frac{e\sigma\mu_c F}{L} \frac{d\tau(t)}{dt} , \quad \mu_c F \tau(t) << L . \tag{24}$$

At longer times, $\mu_c F \tau(t) >> L$, the exponential term may be expanded into a power series and

$$j(t) = \frac{1}{2} \frac{e\sigma L}{\mu_c F [\tau(t)]^2} \frac{d\tau(t)}{dt}, \quad \mu_c F \tau(t) >> L . \tag{25}$$

It is worth noting that the value $\mu_c F \tau(t)$ gives the position of the carrier packet mean, $\langle x \rangle (t)$:

$$\langle x \rangle (t) = \frac{1}{\sigma} \int_0^\infty dx\, x\, p(x,t) = \frac{1}{\mu_c F \tau(t)} \int_0^\infty dx\, x \exp\left[-\frac{x}{\mu_c F \tau(t)} \right] = \mu_c F \tau(t) . \tag{26}$$

Therefore, the crossover from the short-time to the long-time current asymptotes occurs when the packet mean reaches the rear contact. Under the dispersive transport regime, this time is identified as the transit time, t_T: $\langle x \rangle (t_T) = \mu_c F \tau(t_T) = L$.

4.4. Application to a model for a-Si:H

Equation (25) establishes a basis for the post-transit photocurrent analysis. Substituting Eq. (14) into Eq. (25) yields the following relationship between the time dependence of the post-transit photocurrent and the DOS energy distribution:

$$g[kT\ln(\nu_0 t)] = \frac{2\mu_c F\tau_0}{e\sigma L}\frac{N_t}{kT}t\,j(t). \tag{27}$$

This corresponds of course to the relationship given earlier in Eq. (3). In terms of the utilized concept of metastable states, the underlying physics is very simple. Before the thermal equilibrium is established, *i.e.* under the dispersive transport regime, carrier transport kinetics is controlled by the carrier release time from the currently metastable states. In other words, the dispersive carrier transport is always controlled by carrier emission from metastable states. The density of the latter decreases with time as described by Eq. (7), implying an increasing average distance for carriers to cross before being trapped again by a metastable state. At sufficiently long times this distance exceeds the sample thickness and a carrier, once released from a metastable state, will on average leave the sample rather than being retrapped by another metastable state. Under these conditions, the transient current is determined at any given time by the rate of thermal carrier release from those

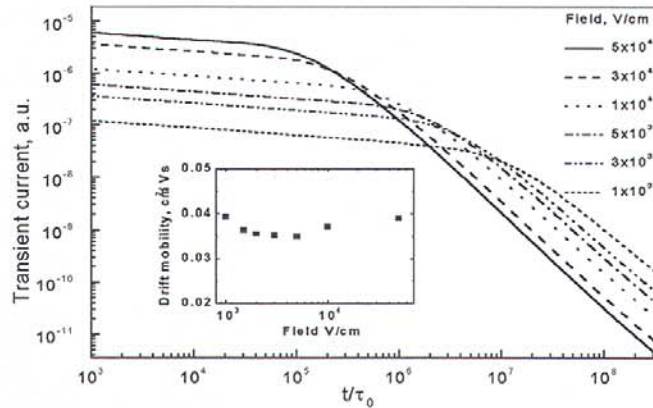

Fig. 6. Influence of the electric field on the calculated time dependence of the transient current in a material with a DOS as described by Eq. (28). The inset illustrates an anomalously weak field dependence of the drift mobility as obtained from the curves. The following parameters were used: $N_t = 10^{21}$ cm^{-3}, $N_d = 10^{15}$ cm^{-3}, $E_t = 0.03$ eV, $\sigma = 0.08$ eV, $E_d = 0.55$ eV, $\tau_0 = 10^{-12}$ s, $\nu_0 = 10^{11}$ s^{-1}, T = 300 K.

traps which cease to be metastable, thus linking the current and the energy distribution of trapped carriers. With the carrier capture cross section assumed to be energy-independent, the energy distribution of carriers localized in metastable states mimics the metastable DOS energy distribution and, therefore, the time dependence of the post-transit transient current allows one to recover a deep tail of the DOS distribution.

In a-Si:H, the DOS distributions on both conduction or valence band sides of the gap can to a good approximation be modeled by the sum of two components. One is a monotonically decreasing tail of states from the mobility edge into the gap and well-described by an exponential function. The second one reflects the deep defect states whose energy distribution can be described by a Gaussian function. The total density of deep states is normally much less than that of band-tail states. Therefore, a realistic expression for the DOS distribution in a-Si:H can be written as

$$g(E) = \frac{N_t}{E_t}\exp\left(-\frac{E}{E_t}\right) + \frac{N_d}{\sqrt{2\pi}\sigma}\exp\left[-\frac{(E-E_d)^2}{2\sigma^2}\right]. \tag{28}$$

Current transients calculated for this DOS function are plotted in Fig. 6, parametric in the electric field. The inset to this figure shows the resolved field dependence of the carrier drift mobility that is calculated from the kinks in the different log *j* *vs* log *t* curves. One can see that, although all *j* *vs*

t curves do reveal typical dispersive shapes, the apparent drift mobility appears to be almost independent of the electric field due to the interplay between carrier transport and trapping by deep localized states. The evolution of the calculated TOF current transients with decreasing temperature is illustrated in Fig. 7. The inset shows that the temperature dependence of the drift mobility does show the expected Arrhenius law similar to the experimentally observed Eq. (2).

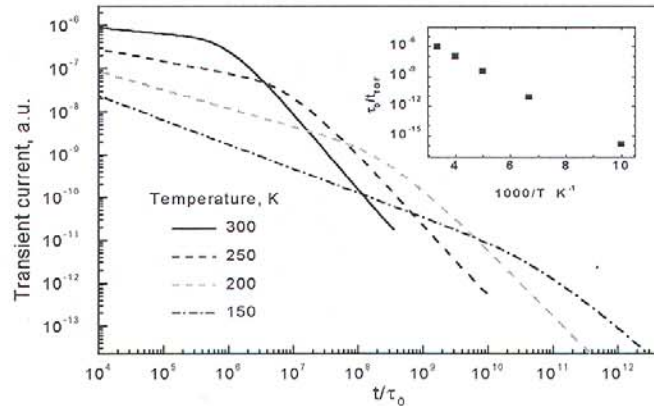

Fig. 7. Temperature dependence of the calculated TOF current transients for the model DOS of Eq. (28). The inset shows an Arrhenius-like temperature dependence of the resolved drift mobility, with an activation energy of 0.30 eV. The model parameters are as in Fig. 6 and $F = 10^4$ V/cm.

5. Summary and conclusions

The analysis of TOF transient photocurrents of a-Si:H prepared in an expanding thermal plasma has shown that this high-deposition-rate technique does produce a-Si:H layers with a higher hole mobility than is found in PECVD material, albeit with a somewhat lower electron mobility. It was further noted that the overall density of localized states does not differ strongly from what is observed in device-quality PECVD samples, but that the distribution may be different in that there apparently is a lower minimum in the DOS between the tail states and the dangling bond defect levels. This makes these deep defects stand out prominently above the background and explain both the occurrence of a pure t^{-1} section in the post-transit current decay and the lack of electric field dependence of the measured drift mobilities. Theoretical analysis and model calculations have indeed demonstrated that such field independence will be observed whenever a prominent deep-trapping component interferes with the multiple-trapping transport process.

Acknowledgements

H.-Z. S. acknowledges a fellowship from the *Fonds voor Wetenschappelijk Onderzoek – Vlaanderen*; V.I. A. and E.V. E. acknowledge research fellowships from the *K. U. Leuven*.

References

[1] R. J. Severens, M. C. M. van de Sanden, H. J. M. Verhoeven, J. Bastiaanssen, D. C. Schram, Mat. Res. Soc. Symp. Proc., **420**, 341 (1996).
[2] B. A. Korevaar, G. J. Adriaenssens, A. H. M. Smets, W. M. M. Kessels, H.-Z. Song, M. C. M. van de Sanden, D. C. Schram, J. Non-Cryst. Solids , in press.

[3] G. J. Adriaenssens, in Amorphous Insulators and Semiconductors, eds. M. F. Thorpe and M. I. Mitkova (Kluwer, Dordrecht, 1997), p. 437.
[4] J. M. Marshall, Rep. Prog. Phys., **46**, 1235 (1983).
[5] T. Tiedje, in The physics of Hydrogenated Amorphous Silicon II, eds. J. D. Joannopoulos and G. Lucovsky (Topics in Applied Physics, vol.56, Springer-Verlag, Berlin, 1984) p. 261.
[6] T. Tiedje, J. M. Cebulka, D. L. Morel, Abeles B., Phys. Rev. Lett., **46,** 1425 (1981).
[7] T. Tiedje, B. Abeles, J. M. Cebulka, Solid State Commun., **47**, 493 (1983).
[8] G. J. Adriaenssens, in Properties of amorphous silicon and its alloys, ed. T. Searle (INSPEC, IEE, London, 1998), p. 199.
[9] G. F. Seynhaeve, R. P. Barclay, G. J. Adriaenssens, J. M. Marshall, Phys. Rev., **B39,** 10196 (1989).
[10] M. Silver, E. Snow, D. Adler, Solid State Commun., **53**, 637 (1985).
[11] B. Yan, G.J. Adriaenssens, J. Appl. Phys., **77**, 5661 (1995).
[12] V. I. Arkhipov, A. I. Rudenko, Sov. Phys. Semicond., **13**, 792 (1979).
[13] V. I. Arkhipov, M. S. Iovu, A. I. Rudenko, S. D. Shutov, phys. stat. sol. (a), **54**, 67 (1979).
[14] J. M. Marshall, J. Berkin, C. Main, Phil. Mag., **B56**, 641 (1987).